Limnol. Oceanogr., 59(5), 2014, 1493–1509
© 2014, by the Association for the Sciences of Limnology and Oceanography, Inc.
doi:10.4319/lo.2014.59.5.1493

Sources and fate of nitrate in a groundwater-fed estuary elucidated using stable isotope ratios of nitrogen and oxygen

Wei Wen Wong,[1,*] Michael R. Grace,[1] Ian Cartwright,[2] and Perran L. M. Cook [1]

[1] Water Studies Centre, School of Chemistry, Monash University, Clayton, Victoria, Australia
[2] School of Geosciences, Monash University, Clayton, Victoria, Australia

Abstract

We used δ^{15}N-nitrate (NO_3^-) and δ^{18}O-NO_3^- to unravel the provenance and fate of NO_3^- in a groundwater-fed estuary. A total of 13 monthly and two time series surveys were undertaken in the Werribee River estuary near Melbourne, Australia. The different survey timescales provided a comprehensive evaluation of the hydrological effects on the biogeochemistry of NO_3^-, which accounted for tidal variability and episodic runoff events. The distribution of δ^{15}N and δ^{18}O of the estuarine NO_3^- along a mixing line between shallow and deep groundwater provided strong evidence for the predominance of groundwater-derived NO_3^- in the estuary. During dry periods when water residence time in the estuary was extended, shallow groundwater contributed 60% to 76% of the NO_3^- (calculated from δ^{15}N-NO_3^- and δ^{18}O-NO_3^-) to the estuary, and assimilation removed ~ 70% of this groundwater-derived NO_3^-. During wet periods, deep groundwater provided more (62%) NO_3^- than shallow groundwater, and there was no indication of NO_3^- consumption. Occasional sources of NO_3^-, which were also reflected by their δ^{15}N-NO_3^- and δ^{18}O-NO_3^- values, included NO_3^- from nitrification and sewage-derived NO_3^- particularly at the bay entrance to the estuary. Greater emphasis should be placed upon the role of groundwater as a substantial NO_3^- end member when assessing NO_3^- biogeochemistry using methods relying on the dual isotopic composition of NO_3^-.

As an ecotone that connects riverine, marine, and subsurface environments, estuaries play an important role in regulating the fate of nitrogen (N) within these three systems. Estuaries are able to effectively retain and recycle nitrogen through processes such as denitrification and via phytoplankton assimilation (Heiskanen et al. 1998; Middelburg and Nieuwenhuize 2001; Dong et al. 2006). The nitrate (NO_3^-) removal capability of the estuary, however, is commonly overwhelmed by extensive reactive nitrogen loading from growing urbanization and intense agricultural activities near coastal areas. These activities have at least doubled the amount of bioavailable N entering aquatic ecosystems (Galloway 2005), particularly in the form of NO_3^-. Consequently, eutrophication has become the largest contemporary threat to estuaries (Nixon 1995; Kennish 2002). The cascading effects of eutrophication, ranging from algal blooms (Paerl 1997) to the development of hypoxia or anoxia, which in turn leads to damage of sensitive aquatic biota (Paerl et al. 1998), are well documented.

In order to alleviate or constrain the adverse environmental and ecological effects of over-enrichment of NO_3^- in estuaries, tracing and quantifying the sources of NO_3^- are of utmost importance, particularly in setting runoff targets and guidelines for better management of coastal environments (Xue et al. 2009). Nevertheless, understanding the interactions between NO_3^- loading and the attenuation processes of NO_3^- within the hydrodynamic regime of an estuary remains of fundamental interest to many estuarine researchers (Wankel et al. 2006). The combined use of δ^{15}N-NO_3^- and δ^{18}O-NO_3^- has proven to be a powerful tool to simultaneously identify and quantify NO_3^- sources as well as internal turnover processes of NO_3^- in estuaries (Middelburg and Nieuwenhuize 2001; Dähnke et al. 2008; Wankel et al. 2009). This characterization is possible because different sources of NO_3^- commonly exhibit distinct isotopic signatures, while the biological processing of NO_3^- has predictable fractionation factors (Kendall et al. 2007) as a result of preferential consumption of $^{14}NO_3^-$ over $^{15}NO_3^-$.

Previous estuarine studies have utilized the dual isotopic technique to account for NO_3^- contribution from riverine discharge (Dähnke et al. 2008), to indicate the occurrence of nitrification (Sebilo et al. 2004), and to estimate the relative importance of a specific diffuse source, for instance, sewage discharge (Wankel et al. 2006). However, very few studies have looked at the applicability of δ^{15}N-NO_3^- and δ^{18}O-NO_3^- to tracking and apportioning the contribution of groundwater-derived NO_3^-, which enters the estuary via submarine groundwater discharge (SGD). Null et al. (2012), for example, used δ^{15}N-NO_3^- and δ^{18}O-NO_3^- in the San Francisco Bay to show that recirculated seawater was the primary component of SGD to the South Bay. Their study concluded that δ^{15}N-NO_3^- and δ^{18}O-NO_3^- could be important proxies to delineate the relationship between the surface and the groundwaters.

SGD is increasingly seen as an important conduit delivering terrestrial NO_3^- to estuaries because the NO_3^- concentration in groundwater is commonly much higher than in surface waters (Burnett and Dulaiova 2003; Slomp and Van Cappellen 2004; Santos et al. 2010). SGD may comprise isotopically modified primary sources of NO_3^- (e.g., fertilizer and sewage) as a result of the possible active biogeochemical processes (i.e., denitrification) in the subsurface environment, including the subterranean estuary and the riparian zone (Kroeger and Charette 2008;

* Corresponding author: weiwen.wong@monash.edu

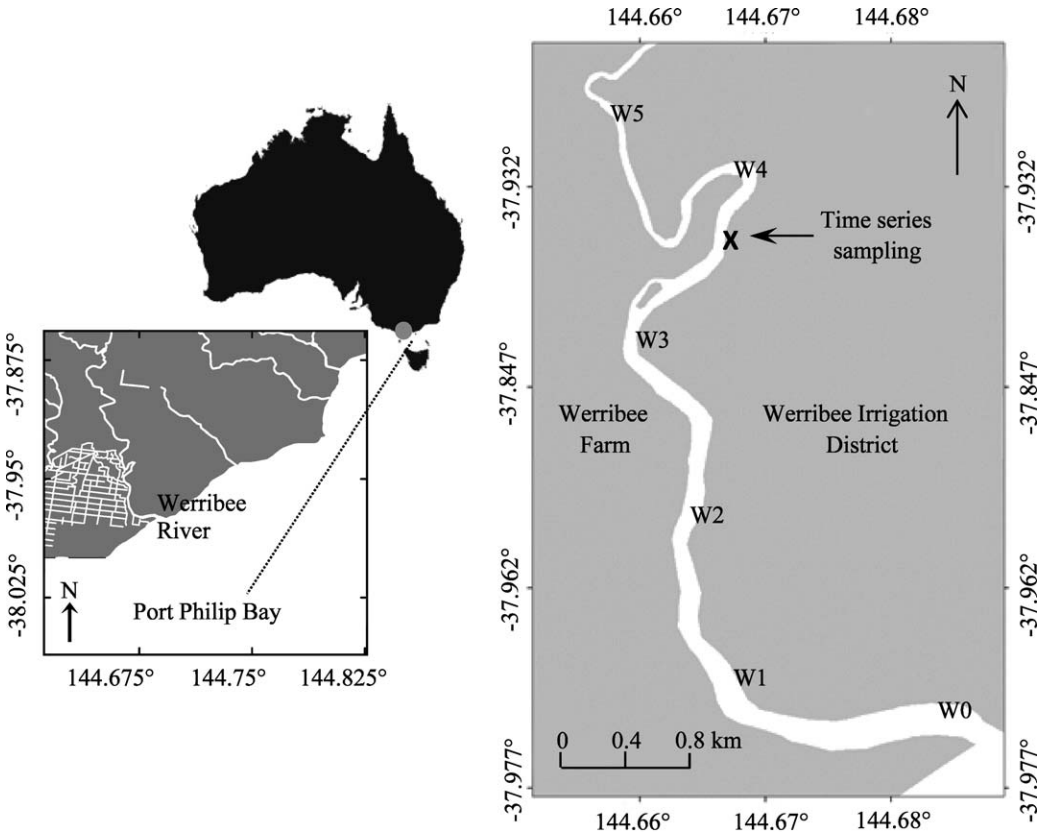

Fig. 1. Map of the Werribee River estuary in southern Victoria, Australia. W0 to W5 represent monthly point sampling sites, the cross represents the location at which groundwater samples were obtained, and the arrow represents the moored time series sampling site.

Santos et al. 2009). Depending on the degree of isotopic fractionation, the isotopically modified primary sources may not be correctly identified using the initial isotopic signatures of the primary sources. Hence, the failure to account for the contribution of SGD in quantifying the actual sources of NO_3^- to estuaries may lead to inaccurate estimation of the percentage contribution of the primary sources. The key question driving this study is this: *If the SGD rate is relatively well constrained, can* $\delta^{15}N\text{-}NO_3^-$ *and* $\delta^{18}O\text{-}NO_3^-$ *be examined to discriminate between the effects of subsurface discharge and surface runoff in order to more accurately estimate the overall contribution of a particular source of* NO_3^-*?* This concept is investigated in a eutrophic, groundwater-fed estuary in southern Victoria, Australia—the Werribee River estuary.

The Werribee River estuary is surrounded by two conspicuous sources of surface NO_3^-—fertilizer from extensive horticulture activities in the Werribee Irrigation District and sewage from the Werribee Farm and Western Treatment Plant (Fig. 1). Because of these obvious sources, the elevated NO_3^- concentrations in the estuary were often presumed to have originated from surface runoff (A. R. Longmore unpubl.). However, Wong et al. (2013) have shown that SGD contributes a significant amount of NO_3^- into the estuary; NO_3^- in shallow groundwater (depth between 0.5 m and 5 m) originated entirely from fertilizer, while deep groundwater (depth between 15 m and 20 m) contained 69% sewage-derived NO_3^- and 31% fertilizer-derived NO_3^- (W. W. Wong unpubl.). This finding adds another layer of complexity to the efforts to determine the major sources of NO_3^- to the Werribee River estuary. We hypothesized that as long as NO_3^- in the two groundwater sources has distinctive isotopic signatures, the relative NO_3^- contribution of shallow and deep groundwater to the estuary can be determined.

This study was conducted from April 2010 to April 2011 and focused on addressing three major questions: (1) Can isotopic values of NO_3^- track the groundwater-derived NO_3^- and be distinguished from other sources in a dynamic estuarine system? (2) What are the major sources of NO_3^- to the Werribee River estuary and how do these sources of NO_3^- vary spatially and temporally on hourly to monthly timescales? (3) Is NO_3^- assimilation or uptake an important process in controlling the availability of NO_3^- in the estuary and how is such uptake affected by the hydrology of the estuary?

Methods

Site description and study site—The Werribee River estuary (Fig. 1) is a shallow, salt wedge estuary located ~ 37 km west of Melbourne, Victoria, Australia. The site is one of three major estuaries discharging into Port Philip Bay, a nitrogen-limited coastal embayment (CSIRO 1996).

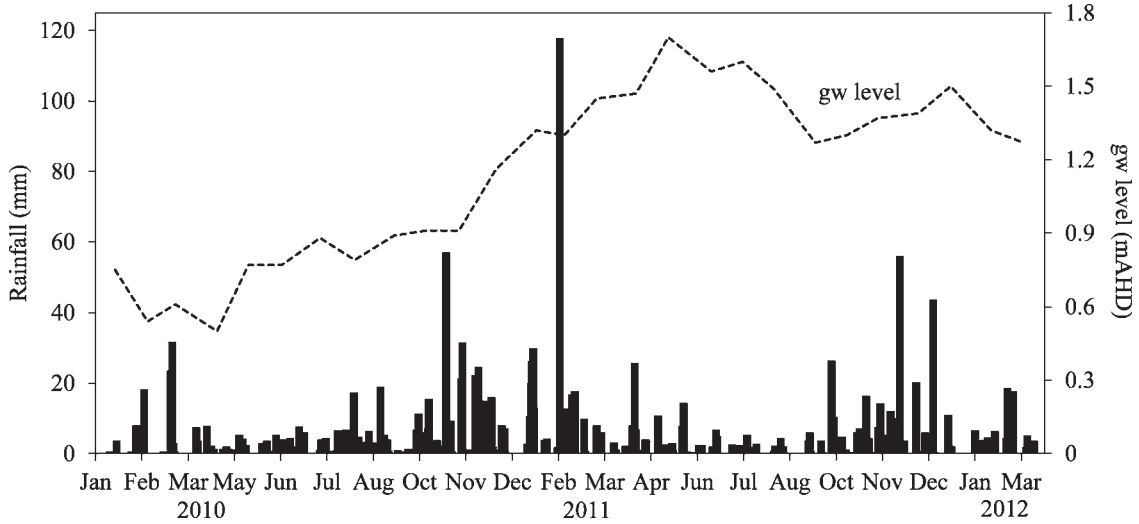

Fig. 2. Daily rainfall (mm) and deep groundwater level (m AHD) data from January 2010 to March 2012.

Agricultural practices dominate ~ 67% of land use in the Werribee catchment, while 25% retains natural vegetation and 5% is urbanized (Melbourne Water Corporation unpubl.). The estuary lies between an irrigation district on the east side and a sewage treatment plant on the west side and extends 8.25 km from Port Philip Bay, with an upstream limit defined by a ford. The average depth of the estuary is ~ 2.0 m, and it has an estimated surface area of 7.16×10^5 m^2. It is subject to the tidal fluctuations of Port Philip Bay, in which the tidal prism is approximately one-third of the estuary volume during low tide (J. Sherwood unpubl.).

The flow of the estuary is through a regulated diversion weir (located about 8.2 km upstream from the ford) and from stormwater drains that enter the estuary from the eastern shore. There are no other tributaries flowing directly into the estuary. SGD was the major source of freshwater to the estuary. The highest groundwater discharge was observed at the reach between W3 and W4 (Fig. 1) during baseflow conditions. From the January 2012 time series survey, the total SGD flux to the estuary of 8240 m^3 d^{-1} (Wong et al. 2013) was greater than freshwater fluxes from other sources (i.e., riverine discharge: 4410 m^3 d^{-1}, rainfall: 1290 m^3 d^{-1}; and recycled water: 5750 m^3 d^{-1}). Thus, in relation to SGD, riverine discharge, recycled water, and rainfall were 52%, 70%, and 16%, respectively, thereby substantiating the importance of SGD as a freshwater source to the estuary.

The Werribee catchment has a temperate climate, with long-term annual rainfall varying from about 1000 mm in the headwaters to as little as 450 mm over the estuary (http://www.bom.gov.au/climate/data/; station number 087031). Monthly mean rainfall in summer (December–February) is higher than during other times of the year. There were 4 months with monthly total rainfall exceeding 60 mm: October and November 2011 and January and February 2012 (Fig. 2). These months are defined as the wet periods in the context of this study.

Sampling and experimental methodology—A total of 13 longitudinal surveys along the salinity gradient of the estuary (Werribee, W0 to W5 in Fig. 1) were conducted monthly between April 2010 and April 2011. During these sampling events, water quality parameters (pH, electrical conductivity, salinity, turbidity, dissolved oxygen [DO] concentration, and water temperature) were measured using a calibrated Horiba U-10 meter. Time series surveys were carried out in March 2011 and January 2012 at the point at which the highest NO_3^- concentrations were observed throughout the preceding monthly survey (W4). For the time series, individual grab samples of the surface and bottom waters were obtained using a pump approximately every hour for 23 h. We also deployed salinity loggers at different water levels (Odyssey Data Recorder) and multi-parameter water quality sondes (Hydrolab DS5X), which recorded measurements of water level, pH, salinity, conductivity, DO, turbidity, and water temperature every 15 min. Multiple samples were also obtained from W5 to represent the riverine input during the time series survey. In earlier surveys during April and September 2008, intact sediment cores at W0, W1, and W2 (Fig. 1) were collected in 30×6.7 cm polycarbonate cylinders and stoppered. Five cores were collected from each site, one for porosity and four for the measurement of sediment fluxes of NO_3^- and NH_4^+. Approximately 10 liters of bottom water was also collected for the sediment incubations.

In addition to the estuarine samples, all potential sources of NO_3^- were collected. These include sewage effluent from the wastewater treatment plant, recycled water used for irrigation of the agricultural farms, total precipitation, shallow and deep groundwater, and sediment from the bottom of the estuary. Deep groundwater samples were collected from a state observation bore adjacent to the estuary using a submersible pump. The screened interval of the bore is between 6 m and 8 m below the bottom of the estuary. Shallow groundwater was collected from manually installed piezometers using a peristaltic pump during the January 2012 survey. Three 1.5 cm diameter stainless-steel piezometers were driven to a depth of 50 cm (screen depths between 30 cm and 50 cm) below the sediment–water interface in the estuary at site W4, along the east bank

below a 5 m cliff. Total precipitation was collected from a rain gauge, which was located at the Werribee Farm on the western side of the estuary. Sewage effluent, which discharges directly to Port Phillip Bay, was obtained from the Western Treatment Plant, while recycled water was provided by the local water authority.

Samples for dissolved inorganic nutrients (DIN; ammonium, NH_4^+; NO_3^-, and nitrite, NO_2^-) and filterable reactive phosphorus (FRP) and δ^{15}N-NO_3^- and δ^{18}O-NO_3^- were filtered through 0.2 μm polypropylene membranes placed in an acid-washed filter holder. Samples for total nitrogen (TN) and δ^{18}O-H_2O were collected directly from the estuary. All samples were stored and transported on ice until they were refrigerated (nutrient samples were frozen) in the laboratory.

Measurements of benthic nutrient flux—Sediment cores were transferred to a temperature-controlled water bath and incubated overnight with site bottom water, at in situ temperature and oxygen concentration. The water column of the sediment core was mixed using a suspended magnetic bar (the stirring rate was kept low to avoid sediment disturbance), and in situ oxygen conditions were maintained by circulating with aerated site bottom water. A time series of four measurements was made over 2–6 h, with the time steps dependent on the rate of oxygen consumption. At each time, DO and pH were measured, and $\sim$ 50 mL of water was collected for the analyses of NO_3^- and NH_4^+. The water sample was pre-filtered through a GF/F filter followed by a 0.22 μm polypropylene membrane and frozen in a 100 mL polypropylene screw-cap bottle. The withdrawn volume of water was replaced with water from the reservoir. The nutrient flux was calculated as

$$\text{flux} = (\alpha - \alpha_W)\frac{V}{A} \quad (1)$$

where α is the linear regression slope of analyte in sediment core (μmol L^{-1} h^{-1}); α_w is the linear regression slope of analyte in the 'blank' core; V is the water column volume (liters); and A is the sediment surface area (m^2).

Measurement of denitrification rate—After the flux incubation, the cores were recirculated with the site bottom water under in situ oxygen and temperature conditions overnight to allow the sediments and water to re-equilibrate. The denitrification rate was measured using the isotope pairing technique of Nielsen (1992). The experiment began with the addition of $^{15}NO_3^-$ (98% +, Cambridge Isotope Laboratories) to each core, with filtered water samples ($\sim$ 15 mL) collected immediately before and immediately after addition. The displaced volume of water was replaced with site bottom water and the core sealed. After approximately 30 min (time 1), 1 mL of $ZnCl_2$ (50% w : v) was added to a single core, which halted further denitrification. This core was then slurried, and a sample was collected in a 12 mL airtight exetainer (Labco) and further preserved with 250 μL of $ZnCl_2$. This was repeated for subsequent cores at time intervals ranging between 30 min and 1.5 h. Samples were analyzed in a gas chromatograph–mass spectrometer (Shimazu GCMS-QP5050) for $^{28}N_2$, $^{29}N_2$, and $^{30}N_2$. Denitrification rate was determined from the linear relationship observed over time with respect to excess ^{15}N-labeled N_2 gas production (Nielsen 1992; Dalsgaard et al. 2000).

Analytical procedure—All chemical analyses were performed within 1–2 weeks of sample collection, except for isotope analyses (performed within 1 month). The concentrations of FRP, DIN, and total dissolved nitrogen (TDN) were determined spectrophotometrically using a Lachat QuikChem 8000 Flow Injection Analyzer (FIA), following standard procedures (APHA 2005). Samples for TN were digested with alkaline persulfate prior to analysis via FIA. Analysis of standard reference materials indicated the accuracy of the spectrophotometric analyses was always within 2% relative error. The samples for δ^{15}N-NO_3^- and δ^{18}O-NO_3^- were analyzed using the bacterial denitrifier method based on procedures outlined in Sigman et al. (2001) at the Colorado Plateau Stable Isotope Laboratory (Arizona). In brief, in this method NO_x (NO_3^- + NO_2^-) is quantitatively converted to N_2O by a strain of denitrifying bacteria that lacks N_2O reductase activity, followed by isotopic analysis of the resultant N_2O by continuous-flow isotope ratio mass spectrometry (CF-IRMS). Nitrogen (δ^{15}N-NO_3^-) and oxygen (δ^{18}O-NO_3^-) isotope ratios are reported in per mil (‰) relative to atmospheric air and Vienna Standard Mean Ocean Water (VSMOW), respectively. The external reproducibility of the isotopic analyses lies within $\pm$ 0.07 for δ^{15}N and within $\pm$ 0.18 for δ^{18}O. The δ^{18}O-H_2O values were measured via equilibration with He-CO_2 at 32°C for 24 to 48 h in a Finnigan MAT Gas Bench and then analyzed using CF-IRMS. The δ^{18}O-H_2O values were referenced to internal laboratory standards, which were calibrated using VSMOW and Standard Light Antarctic Precipitation. Measurement of two sets of triplicate samples in every run showed a precision of < 0.2‰ for δ^{18}O-H_2O.

Estimation of NO_3^- fractions from shallow and deep groundwater—For both monthly and time series surveys, contributions of shallow ($_{sgw}$) and deep ($_{dgw}$) groundwater to the estuarine samples were calculated using a two end-member mixing model, Eq. 2 (modified from Middleburg and Nieuwenhuize 2001):

$$\delta^{15}N_{sample} = \delta^{15}N_{sgw} \times f_{sgw} + \delta^{15}N_{dgw} \times (1 - f_{sgw}) \quad (2)$$

where f_{sgw} is the fraction of shallow groundwater and δ^{15}N is the δ^{15}N-NO_3^- of shallow and deep groundwaters. The occurrence of a NO_3^- consumptive process was evaluated through the relationship between δ^{15}N-NO_3^- and δ^{18}O-NO_3^-: 1 : 1 and 2 : 1 trends of δ^{15}N-NO_3^- vs. δ^{18}O-NO_3^- indicate the possible occurrence of assimilation and denitrification, respectively (Casciotti et al. 2002; Sigman et al. 2003; Granger et al. 2008); and graphical methods: δ^{15}N-NO_3^- vs. 1/[NO_3^-] trends are nonlinear, while δ^{15}N-NO_3^- vs. ln[NO_3^-] trends are linear when a consumption process is present (Mariotti et al. 1988; Kendall et al. 2007). When consumption processes occur, the initial δ^{15}N-NO_3^- is the intercept between the regression lines of the consumption trend and the shallow and deep groundwater mixing line.

To determine the amount of NO_3^- consumed in the estuary (as a fraction of all NO_3^-), the predicted NO_3^- concentration (N) from conservative mixing between the bay and groundwater was first calculated using the following equation (modified from Middelburg and Nieuwenhuize 2001):

$$N_{cm} = \frac{N_m \times (S_{obs} - S_{gw}) + N_{gw} \times (S_m - S_{obs})}{S_m - S_{gw}} \quad (3)$$

where N_{cm}, N_m, and N_{gw} are NO_3^- concentrations predicted from conservative mixing, the marine end member, and NO_3^- concentrations in groundwater, respectively. S denotes salinities of the different components. S_{obs} represents the salinity observed at respective sampling points. The fraction of NO_3^- consumed (F) was then calculated (Eq. 4) as the ratio between the measured NO_3^- concentration and that predicted by Eq. 3:

$$F = 1 - \frac{\text{measured } NO_3^-}{\text{predicted } NO_3^-} \quad (4)$$

The enrichment factor (ε) of the consumption process was approximated from the slope of the linear regression of $\delta^{15}N$ vs. ln(F) (Sigman et al. 1999; Alkhatib et al. 2012), following the Rayleigh equation (Kendall et al. 2007), Eq. 5:

$$\delta^{15}N = \varepsilon \ln(F) + \delta^{15}N_i \quad (5)$$

where $\delta^{15}N$ denotes the isotopic value of the measured NO_3^- and $\delta^{15}N_i$ is the predicted isotopic value of the initial NO_3^- before being consumed (the intercept of the sgw–dgw mixing line and the assimilation trend).

Results

Monthly survey of the estuary (W0–W5)—Physicochemical characteristics: Salinities of the water column ranged from near seawater (33) at W0 to near freshwater (1.3) at W5. During the wet period (October and November 2010, January and February 2011), the salinity of the water column decreased to approximately 23 at W0, reflecting greater influence from surface runoff, direct precipitation, and/or increased riverine discharge. The estuary was oxic throughout the survey, with an average O_2 concentration of 0.6 ± 0.3 mmol L^{-1}. The high proportion of NO_3^- in DIN (88% ± 10%) and TN (45% ± 25%) suggests not only that NO_3^- was the major form of DIN but that in fact NO_3^- was the main nitrogenous compound in the estuary. In addition, at W3 and W4, NO_3^- comprised > 50% of the TN concentration (except for during the October 2011 survey), reflecting the dominance of this species throughout the course of the survey at these sampling points. As shown in Fig. 3a, the highest NO_3^- concentrations were typically observed at W4 (except during the wet period, October 2010, January 2011, and February 2011). Monthly NO_3^- average concentrations in the lower estuary (W2–W4) were generally greater (98 μmol L^{-1}) than that of the freshwater end member W5 (56 μmol L^{-1}), while that of the bay entrance W0 (50 μmol L^{-1}) was typically lower than those of any sampling point in the estuary (Fig. 3).

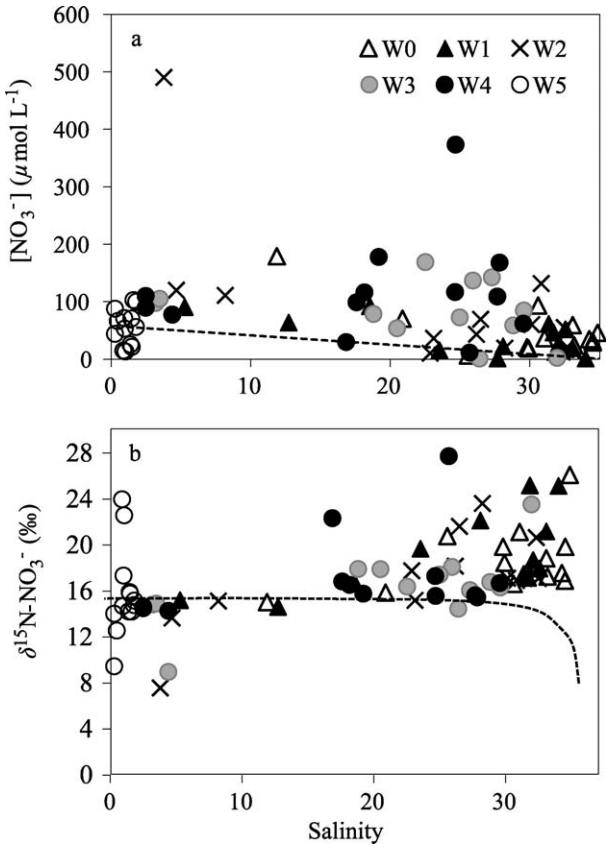

Fig. 3. Relationship between (a) [NO_3^-] (μmol L^{-1}) and salinity and (b) $\delta^{15}N$-NO_3^- (‰) and salinity. The dotted line in (a) represents the theoretical mixing line between the NO_3^- concentration in Port Phillip Bay and the average NO_3^- concentration of the riverine input (W5) and in (b) the conservative mixing line between the $\delta^{15}N$-NO_3^- of the bay (assuming $\delta^{15}N$-NO_3^- of the southern ocean to be +8‰; Lourey et al. 2003) and the average $\delta^{15}N$-NO_3^- of the river.

The NO_3^--salinity and $\delta^{15}N$-NO_3^--salinity mixing diagrams (Fig. 3a and b, respectively) of all the estuarine samples showed non-conservative behavior, with most of the NO_3^- concentrations and $\delta^{15}N$-NO_3^- values falling above the river–bay mixing line (represented as a dotted line in Fig. 3). This also suggests that riverine NO_3^- was not the dominant source of NO_3^- to the estuary. The NO_3^--salinity mixing line was set based on the average salinity, NO_3^- concentrations, and $\delta^{15}N$-NO_3^- at site W5 as the freshwater end member. The salinity value of Port Philip Bay as the marine end member (35.4) was taken from http://www.metoc.gov.au/products/data/aussss.php?search&Melbourne, while the NO_3^- concentration of 0.4 μmol L^{-1} was obtained from Ellis et al. (2011). We did not measure the $\delta^{15}N$-NO_3^- of the Bay but rather adopted a value of 8‰, the $\delta^{15}N$-NO_3^- value reported for the Southern Ocean (Lourey et al. 2003).

Distribution of NO_3^- isotopic composition: The $\delta^{15}N$-NO_3^- of the estuarine samples (from +15‰ to +28‰) was typically higher than that of the freshwater samples (W5: +16‰; Fig. 4). Among the estuarine samples, $\delta^{15}N$-NO_3^-

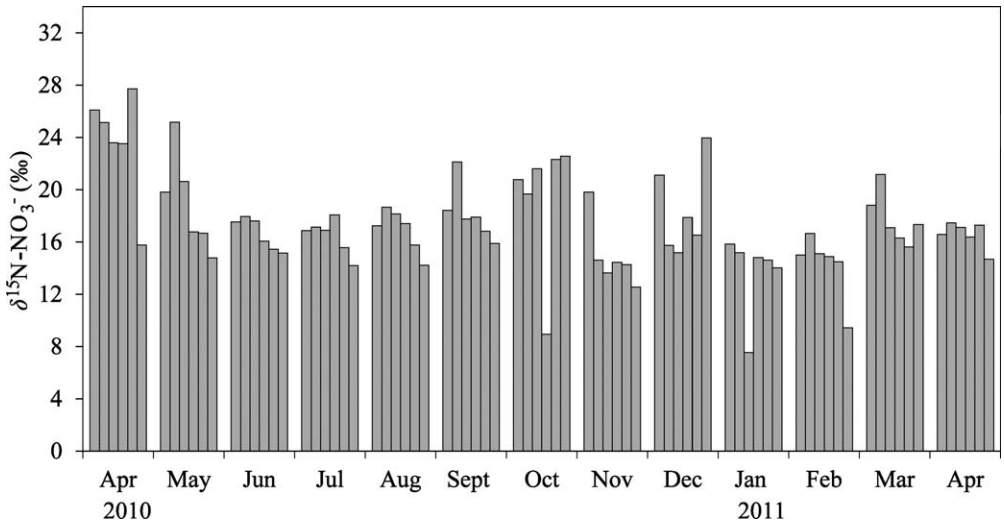

Fig. 4. Spatial and temporal variation of δ^{15}N-NO_3^- values. For each month, sites are ordered W0 to W5.

values at site W4 were relatively more depleted compared to downstream samples (Fig. 4) and were at least 2‰ higher than the average shallow groundwater signature. The spatial trend of δ^{15}N-NO_3^- values was tested using general linear model analysis implemented using the Statistics Analysis Software SAS version 9.3. In the analysis, 'month' and 'site' were included as fixed effects; 'site' was considered as a continuous spatial variable that ranged from downstream (W0) to upstream (W4). In the model, months with high recycled water supply (April and October 2010) and site W5 were excluded to eliminate the effects of recycled water and the freshwater end member, respectively. A significant negative relationship was found (slope = -0.63, $p = 0.0011$) between 'δ^{15}N-NO_3^-' and 'site,' suggesting that δ^{15}N-NO_3^- values decreased from the estuary mouth at W0 to its head at W4, therefore supporting the contention that δ^{15}N-NO_3^- at W4 was relatively more depleted compared to values at the downstream sites. In general, δ^{15}N-NO_3^- was higher during dry periods compared to the wet periods, and heavier δ^{15}N-NO_3^- corresponded with lower NO_3^- concentrations (Fig. 3). The most depleted δ^{15}N-NO_3^- ($< +10$‰) observed in the lower estuary was coincident with the large decrease in salinity (from $\sim$ 20 to 4), indicating localized runoff derived from heavy rainfall. During the April 2010 and October 2010 surveys, the estuarine NO_3^- had an average δ^{15}N-NO_3^- of $>$ 23‰ (Fig. 4). The δ^{15}N-NO_3^- in the bottom water was consistently 2‰ higher compared to that in the corresponding surface water. The distribution of δ^{18}O-NO_3^- was analogous to the δ^{15}N-NO_3^-.

Time series survey of the groundwater discharge hotspot (between W3 and W4)—Physicochemical characteristics: To assess the contribution of groundwater NO_3^- to estuarine NO_3^- concentrations, two time series surveys were undertaken: one in March 2011 and another in January 2012 at the groundwater discharge hotspot, the reach between W3 and W4 (Wong et al. 2013). Observations from the time series surveys are presented in Fig. 5. During the March 2011 survey, the return of the salt wedge after high riverine discharge (average discharge for 21 d prior to sampling: 250 $\pm$ 1200 ML d^{-1}) resulted in a more stratified system. Salinity of the surface water ranged between 6 and 28, while salinity of the bottom water ranged between 6 and 32 (Fig. 5a). During the January 2012 survey, the estuary was partially mixed, with salinity differences of 7‰ (Fig. 5g) between the surface and the bottom water as a result of prolonged ($\sim$ 21 d) baseflow conditions (10 $\pm$ 34 ML d^{-1}). The groundwater discharge hotspot was influenced by both the river input and tidal fluctuation. During the flood tide, the salinity of the water column was generally higher than through the ebb tide. Little variation was observed for both dissolved oxygen concentration (0.4 $\pm$ 0.1 mmol L^{-1}) and pH (7.8 $\pm$ 0.2).

On the March 2011 survey, the highest NO_3^- concentrations for both surface (125 μmol L^{-1}) and bottom (114 μmol L^{-1}) waters were observed during the second high tide (Fig. 5b). While FRP (5 $\pm$ 2 μmol L^{-1}) showed a similar pattern as NO_3^- with the tide (Fig. 5b), NH_4^+ (8.0 $\pm$ 1.7 μmol L^{-1}) did not show any apparent pattern (Fig. 5c). The upstream nutrient concentrations, representing the riverine input, were almost constant, with NO_3^-, NH_4^+, and FRP concentrations ranging between 79 $\pm$ 6, 8.3 $\pm$ 0.9, and 1.1 $\pm$ 0.2 μmol L^{-1}, respectively. Nutrient concentrations during the January 2012 survey were similar to those of the earlier survey in March 2011. Riverine nutrients at W5 fell within a similar range (NO_3^-: 63 $\pm$ 1 μmol L^{-1}; NH_4^+: 10 $\pm$ 6 μmol L^{-1}; FRP: 1.8 $\pm$ 0.2 μmol L^{-1}). Interestingly, there was a distinctive NO_3^- concentration difference between surface (94 $\pm$ 17 μmol L^{-1}) and bottom water (34 $\pm$ 27 μmol L^{-1}) of the estuary during the January 2012 survey (Fig. 5h). The NO_3^- concentration of the bottom water appeared to be influenced by the tidal fluctuation (based on the significant correlation between the NO_3^- concentration and the salinity of the bottom water, as shown in Fig. 6f), while the tidal effect on NO_3^- concentration was not obvious in the surface water.

Distribution of NO_3^- isotopic composition: The δ^{15}N-NO_3^- values varied from +15.3‰ to +20.8‰ and from +14.2‰ to +17.4‰ for the March 2011 (Fig. 5e) and

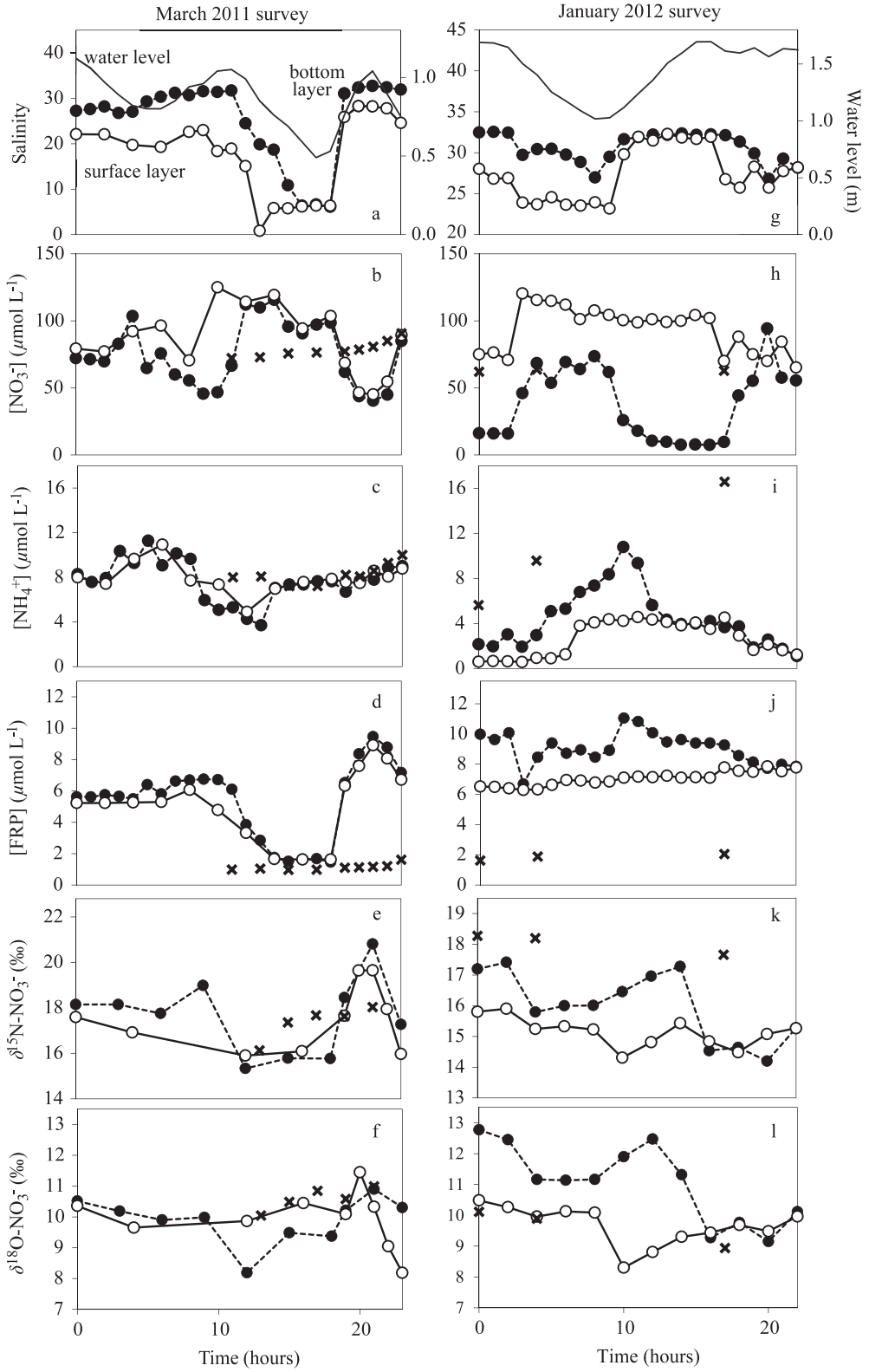

Fig. 5. Observations from time series sampling stations in the Werribee River estuary showing (a,g) salinity; (b,h) NO_3^- concentrations; (c,i) NH_4^+ concentrations; (d,j) FRP concentrations; (e,k) δ^{15}N-NO_3^-; and (f,l) δ^{18}O-NO_3^- in the surface (open circles) and bottom (closed circles) waters at the groundwater discharge hotspot. The crosses represent upstream (U/S) samples from W5, and solid lines in (a) and (g) represent water level.

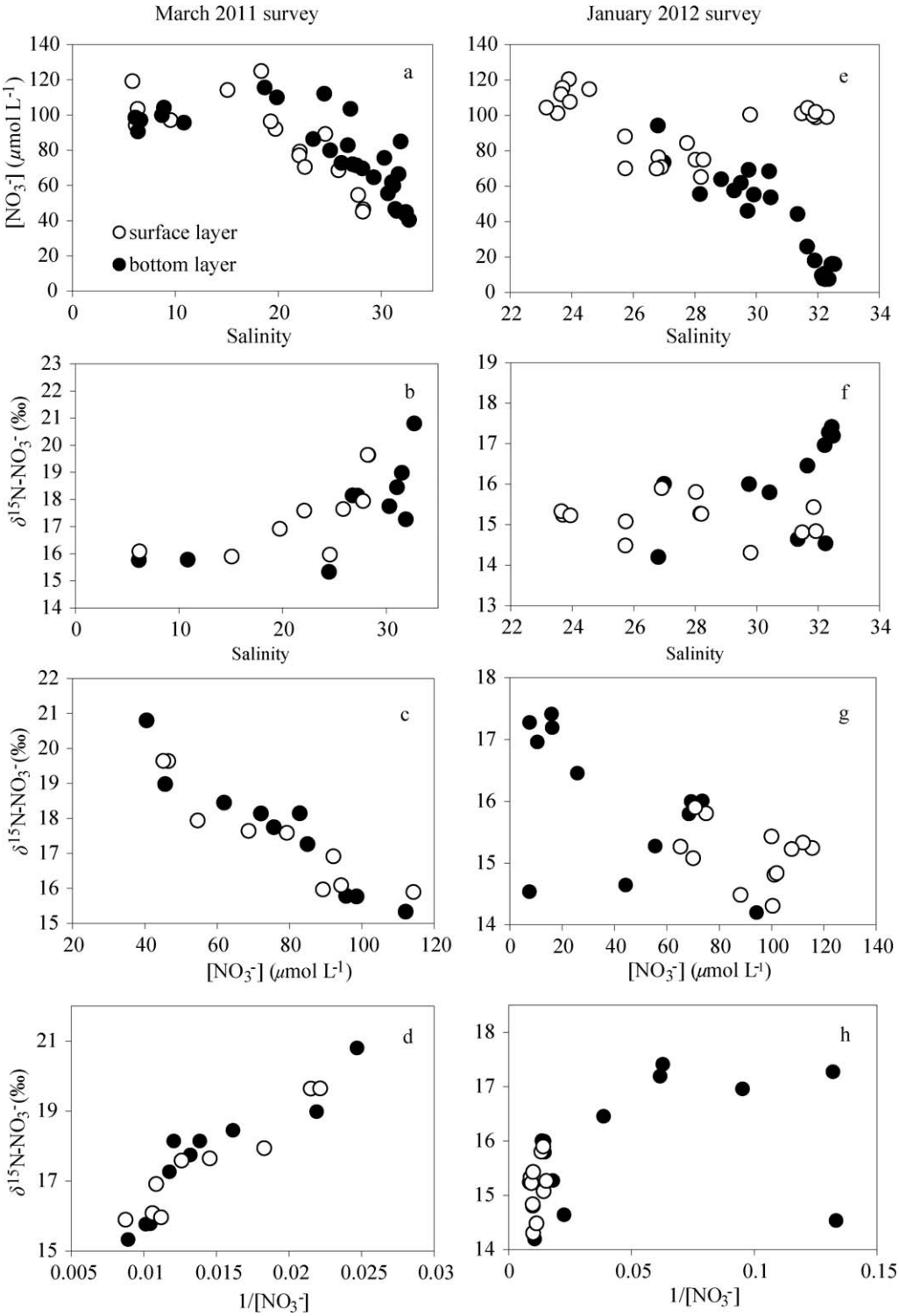

Fig. 6. Relationship between (a, e) NO_3^- (μmol L^{-1}) and salinity; (b, f) δ^{15}N-NO_3^- (‰) and salinity; (c, g) δ^{15}N-NO_3^- and NO_3^- concentration; and (d, h) δ^{15}N-NO_3^- and the reciprocal of NO_3^- concentrations for the March 2011 and January 2012 time series surveys.

January 2012 (Fig. 5k) surveys, respectively. During the two surveys, comparable values of δ^{15}N-NO_3^- were found in the bottom water (March 2011: +17.6 ± 1.7‰; January 2012: +16.0 ± 1.0‰) and in the surface water (March 2011: +17.5 ± 1.4‰; January 2012: +15.1 ± 0.5‰). The temporal distribution of the isotope values followed the salinity of the estuary, except in the case of the δ^{15}N-NO_3^- of the surface water during the January 2012 survey. Relatively higher δ^{15}N-NO_3^- was observed during flood tide compared to ebb tide, while δ^{18}O-NO_3^- showed the opposite

Table 1. Summary of nutrient fluxes and denitrification rate in core incubations.

Survey	April 2008*	September 2008*	Average†	% from gw NO_3^- fluxes‡
Benthic denitrification rate (μmol m^{-2} h^{-1})	70±40	160±40	120±60	3
Benthic NO_3^- flux (μmol m^{-2} h^{-1})	−200±300	−130±80	−170±50	—
Benthic NH_4^+ flux (μmol m^{-2} h^{-1})	700±310	570±640	650±110	9

Negative fluxes denote sediment uptake and positive fluxes denote sediment efflux.
* Means and standard deviations from all three sites, W0, W1, and W3. Standard deviation represents variation between sites.
† Means and standard deviations from the two surveys; April and September 2008.
‡ % of the mean NH_4^+ fluxes and denitrification rate from groundwater (gw) NO_3^- fluxes during a dry period (7.0 mmol m^{-2} h^{-1}).

trend. The δ^{15}N-NO_3^- of the March 2011 survey was significantly correlated with salinity ($r^2 = 0.50$, $p < 0.001$, $n = 19$) as well as NO_3^- concentration ($r^2 = 0.87$, $p < 0.001$, $n = 19$), regardless of the tidal cycle, but δ^{15}N-NO_3^- of the January 2012 survey did not show similar relationships (Fig. 5).

Benthic nutrient flux and denitrification rate—Fluxes of NO_3^- were generally directed into the sediments on both April and September 2008 surveys, with an average flux of 170 μmol m^{-2} h^{-1} (Table 1). Fluxes of NH_4^+ displayed an opposite trend, with a net efflux of 700 μmol m^{-2} h^{-1}. There was a high degree of spatial variability between (as indicated by the standard deviation for each survey in Table 1) and within sites (50–200 μmol m^{-2} h^{-1}; data not shown) for both NO_3^- and NH_4^+ fluxes. Benthic denitrification rates ranged between 70 and 160 μmol m^{-2} h^{-1}, with the higher rate observed during spring (September 2008) rather than autumn (April 2008).

Potential sources of nitrate—Based on predictions from surrounding land use, there are six potential sources that could contribute NO_3^- to the estuary. The possible sources are recycled water used for irrigation, total atmospheric deposition, groundwater, treated-effluent discharge from the wastewater treatment plant, nitrification of NH_4^+ derived from sediment organic matter (SOM) decay, and surface runoff, which comprised modified fertilizer. The concentrations, isotopic compositions of NO_3^-, and δ^{18}O-H_2O for these six sources (which provide the end members for modeling) are summarized in Table 2. The contribution of marine NO_3^- was considered insignificant in this study based on the very low NO_3^- concentration in comparison to other end members and the NO_3^- concentration in the estuary.

Both recycled water and effluent discharge were of sewage origin. Recycled water is used for irrigation of the Werribee Irrigation District (WID), while effluent is discharged to the bay. During the course of the study (April 2010 to April 2011), the amount of recycled water supplied to the study area was ~ 2540 ML, equivalent to 19% of the total rainfall (613 mm) over the area (2150 ha). The highest supplies of recycled water were recorded in April 2010 (828 ML) and October 2010 (457 ML), coinciding with elevated δ^{15}N-NO_3^- of the estuarine NO_3^-.

The groundwater end members comprised two components—shallow groundwater and the deeper groundwater further inland. These two groundwater parcels are comparable in NO_3^- concentration (~ 1.8 mmol L^{-1}) but distinctive in their isotope values, with δ^{15}N-NO_3^- of +21‰ and +12‰ for deep and shallow groundwater, respectively. Shallow groundwater NO_3^- was derived entirely from agricultural sources (fertilizer and recycled water), while the deep groundwater comprised 31% fertilizer and 69% sewage (W. W. Wong unpubl.). Higher groundwater discharge was reported during the January 2012 survey compared to the March 2011 survey (Wong et al. 2013).

The δ^{15}N of the TN in the sediment ranged between +16‰ and +17.5‰. As mineralization of organic matter and subsequent nitrification commonly retain the isotopic value of the SOM or a few per mil difference in δ^{15}N from that of the total organic N in sediment (Kendall et al. 2007), we would expect δ^{15}N-NO_3^- from the nitrification of sediment-derived NH_4^+ to have a value near +16.8‰. Meanwhile, the δ^{18}O-NO_3^- is dependent on the δ^{18}O of the

Table 2. The NO_3^- concentration and the isotopic ratio of NO_3^- as well as H_2O of the putative NO_3^- end members. Values in parentheses are standard deviations based on multiple surveys (n), with $n > 6$.

End member	[NO_3^-] (μmol L^{-1})	δ^{15}N-NO_3^- (‰)	δ^{18}O-NO_3^- (‰)	δ^{18}O-H_2O (‰)
Recycled water	2800 (1900)	+29 (3)	+10.0 (0.4)	−4.9 (0.2)
Treated effluent	1000 (400)	+20 (4)	+6.1 (2.0)	−4.4 (1.0)
Shallow groundwater	1810 (170)	+12.0 (0.4)	+8.2 (0.1)	−3.0 (0.5)
Deep groundwater	1001 (169)	+21.0 (0.7)	+11 (0.9)	−3.35 (0.35)
Total precipitation	7.7 (2.4)	−0.79 (3.03)	+62 (5.4)	−6.05 (0.37)
Nitrification	—	+16.8 (0.5)	+1.12 (0.3)	—
Marine input	0.4	+8*	—	—

* δ^{15}N-NO_3^- of the southern ocean reported by Lourey et al. (2003).

ambient water and $\delta^{18}O$ of the atmospheric oxygen (O_2). The $\delta^{18}O$-NO_3^- value is estimated based on Eq. 6, defined by Casciotti et al. (2002):

$$\delta^{18}O-NO_3^- = \frac{5}{6}\delta^{18}O-H_2O + \frac{1}{6}\delta^{18}O-O_2 \qquad (6)$$

Applying the above equation, the $\delta^{18}O$ of NO_3^- originating from nitrification in this study is +2.7‰, using an average value of −1.46‰ for $\delta^{18}O$-H_2O of the estuarine surface water and a value of +23.5‰ for $\delta^{18}O$-O_2 (Kroopnick and Craig 1972). The use of +23.5‰ as the value of $\delta^{18}O$-O_2 to calculate the $\delta^{18}O$ of NO_3^- produced from nitrification is based on saturation of dissolved oxygen in the estuary. Because dissolved oxygen was rarely undersaturated throughout the course of our study, $\delta^{18}O$-O_2 should range between atmospheric equilibrium (+23.5%) and potentially lower values (< +23.5‰) caused by photosynthesis (Quay et al. 1995; Brandes et al. 1998). As such, +23.5‰ represents the maximum $\delta^{18}O$-O_2 used to calculate the $\delta^{18}O$ of nitrified NO_3^- and thus the maximum estimate of percentage contribution of nitrification to the NO_3^- dynamics in the estuary. Any values < +23.5‰ used in this calculation will result in a lower percentage contribution of nitrification in comparison to other NO_3^- sources.

Discussion

General behavior of NO_3^- in the estuary—The NO_3^- and $\delta^{15}N$-NO_3^--salinity relationship suggests two broad modes of non-conservative behavior of estuarine NO_3^- (Fig. 7). The most common mode is the existence of a NO_3^- spike at the groundwater discharge hotspot (W4), with subsequent NO_3^- consumption downstream of W4. This mode of behavior is observed during dry periods, when most of the NO_3^- concentrations were distributed below the bay–W4 mixing line. The longitudinal decline of NO_3^- concentrations toward the bay from W4, coinciding with increasing $\delta^{15}N$-NO_3^-, demonstrates strong evidence for NO_3^- processing in the Werribee River estuary. The second mode of behavior was the presence of additional sources of NO_3^- during wet periods (November 2010, January and February 2011) and the April 2010 survey (shaded plots in Fig. 7). This mode of behavior is manifest in the positive deviation of the NO_3^- concentration from the bay–W4 mixing line.

The complex interactions between the different modes of NO_3^- behavior were reflected by the isotopic signature of NO_3^- in the Werribee River estuary. Careful inspection of a NO_3^- isotope bi-plot (Fig. 8), and also our knowledge of the local groundwater system and antecedent weather, enable us to interpret the isotope patterns observed as well as to apportion the contribution of different sources to the estuary. The NO_3^- isotope bi-plot (Fig. 8) suggests that (1) The dominant source of NO_3^- is a mixture between what we have termed shallow and deep groundwater, indicated by the solid-red mixing line (Fig. 8). The influence of nitrification on sediment-derived NH_4^+ as well as effluent is also evident, which periodically drags the data points below the deep and shallow groundwater mixing line; (2) There is a sporadic influence of precipitation + fertilizer sources and recycled water coincident with high rainfall and recycled water use, respectively; and (3) During periods of high residence time (low flow periods) there is clear transformation of the NO_3^- isotope signature along the dashed line, termed the assimilation trend (Fig. 8). These three observations are discussed further in the following sections.

Groundwater as the primary source of NO_3^- to the estuary—It has previously been shown that the NO_3^- in the Werribee River estuary predominantly originates from groundwater (Wong et al. 2013). Using the $\delta^{15}N$-NO_3^- and $\delta^{18}O$-NO_3^- data, we are able to gain further insight into the relative importance of different groundwater sources. The distribution of the isotopic ratios of all the sampling events along the mixing line between shallow and deep groundwater (represented by the red solid line in Fig. 8) clearly demonstrated that the estuarine NO_3^- originated from mixing between the two groundwater parcels. Conservative mixing was most notable for the March 2011 survey, during which linear trend lines were observed for the plots of $\delta^{15}N$-NO_3^- vs. $[NO_3^-]$ and $\delta^{15}N$-NO_3^- vs. $1/[NO_3^-]$ (Fig. 6g,h; Kendall et al. 2007).

By manipulating the two end-member mixing model (Eq. 2), the March 2011 survey appeared to mainly comprise deep groundwater (~ 62%). The initial $\delta^{15}N$-NO_3^- and $\delta^{18}O$-NO_3^- values of the January 2012 survey (predicted from the intercept of the sgw–dgw mixing line and the assimilation trend; Fig. 8), on the other hand, indicate a higher percentage of shallow groundwater NO_3^- (~ 76%). The initial $\delta^{15}N$-NO_3^- of the monthly surveys (+15.6‰) also indicates that estuarine NO_3^- contains a higher percentage of shallow (60%) to deep groundwater (40%), suggesting that NO_3^- input from shallow groundwater into the estuary could be equally important over a longer timescale. The apparent difference in the proportions of shallow and deep groundwater NO_3^- between March 2011 and January 2012 surveys suggests the importance of ephemeral hydrological effects on the pathways of SGD to the estuary. We speculate that the differences reflect the combined effects of the change in the lateral shallow subsurface flow and the antecedent hydrological characteristics of the estuary. We note that both time series surveys were carried out when the estuary was under baseflow conditions, which suggests that any influence from the riverine discharge was consistent, and, therefore, fluctuations in the $\delta^{15}N$-NO_3^- signal may largely be attributed to the rate of groundwater discharge and tidal fluctuation.

The March 2011 survey was undertaken in a wet summer (October 2010 to February 2011) with total rainfall of 580 mm and monthly average rainfall of 120 mm. This wet summer occurred after a prolonged low-rainfall period (e.g., 160 mm rainfall over the previous summer, October 2009 to February 2010). During the wet period, groundwater recharge resulted in an increase in the elevation of the water table by ~ 0.4 m over the course of 5 months (Fig. 2). The higher hydraulic gradients between the deep groundwater and the estuary could have increased the discharge of deeper groundwater into the estuary during that period. Hence, $\delta^{15}N$ values of the estuarine NO_3^-

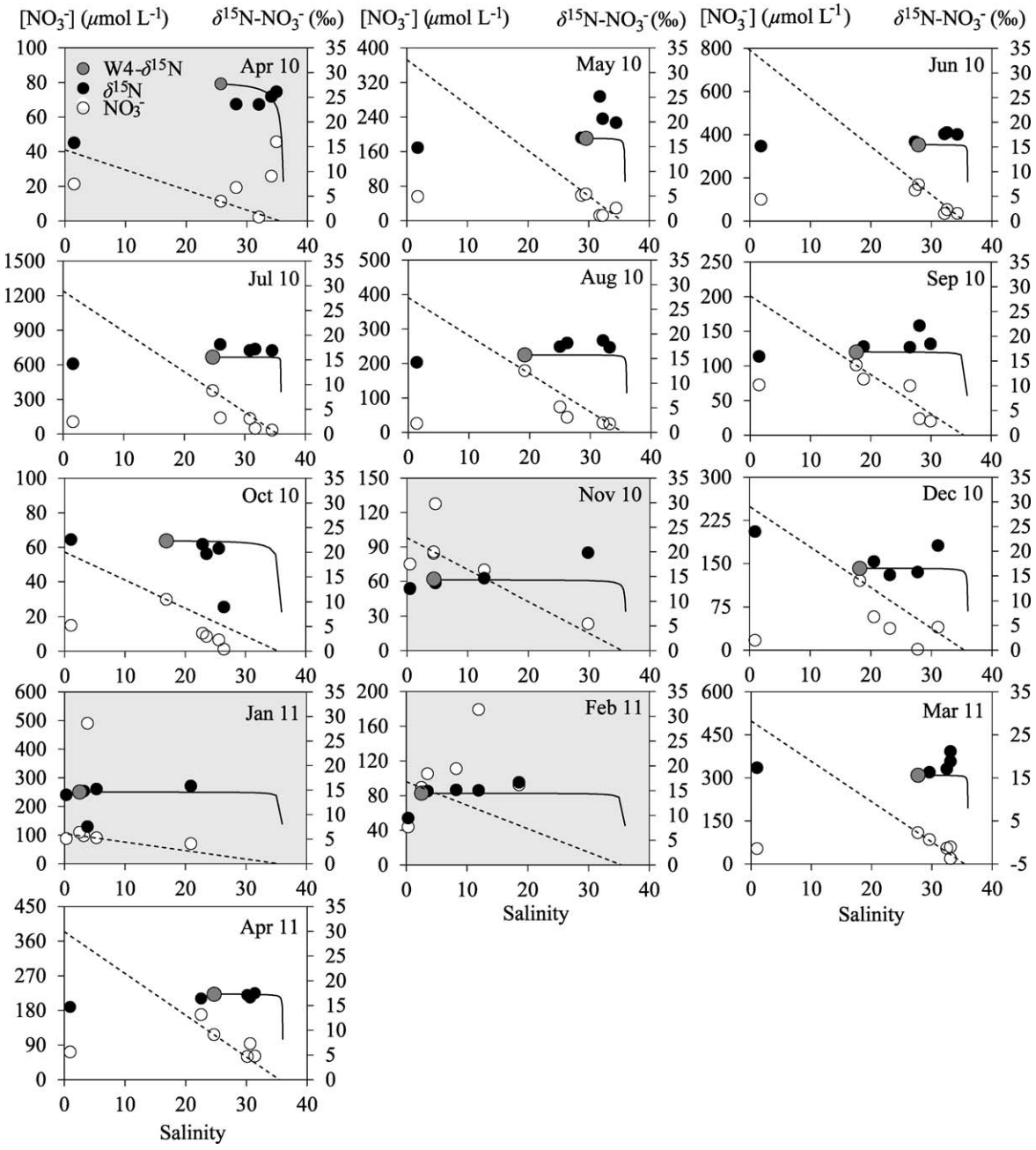

Fig. 7. Nitrate concentration ($[NO_3^-]$) vs. salinity mixing plots for the monthly surveys. Shaded plots indicate the possible occurrence of a NO_3^- production process or the presence of an additional NO_3^- source. The non-shaded plots show the possible presence of a NO_3^- consumption process. Dotted lines represent the conservative mixing line between $[NO_3^-]$ in Port Phillip Bay and W4, the groundwater discharge hotspot. Solid lines represent the conservative mixing between $\delta^{15}N\text{-}NO_3^-$ of the bay (assumed to be 8‰; Lourey et al. 2003) and $\delta^{15}N\text{-}NO_3^-$ of W4.

during this period primarily resembled the signature of the deep groundwater.

In contrast to March 2011, lateral local shallow groundwater flow was the main source of groundwater-derived NO_3^- during the January 2012 survey, as substantiated by the lower deep groundwater level (~ 1.3 m Australian Height Datum [AHD] compared to ~ 1.5 m AHD during March 2011; Fig. 2) and the $\delta^{15}N$ signatures of the estuarine NO_3^-. The relationship between the proportion of deep to shallow groundwater discharge and the intensity of rainfall appears to be counterintuitive. The connectivity of the aquifers in this region is complex and poorly characterized. We speculate that the higher proportion of deep to shallow groundwater during high rainfall event is due to the greater connectivity between the deeper aquifer and the surface water in the zones of recharge than

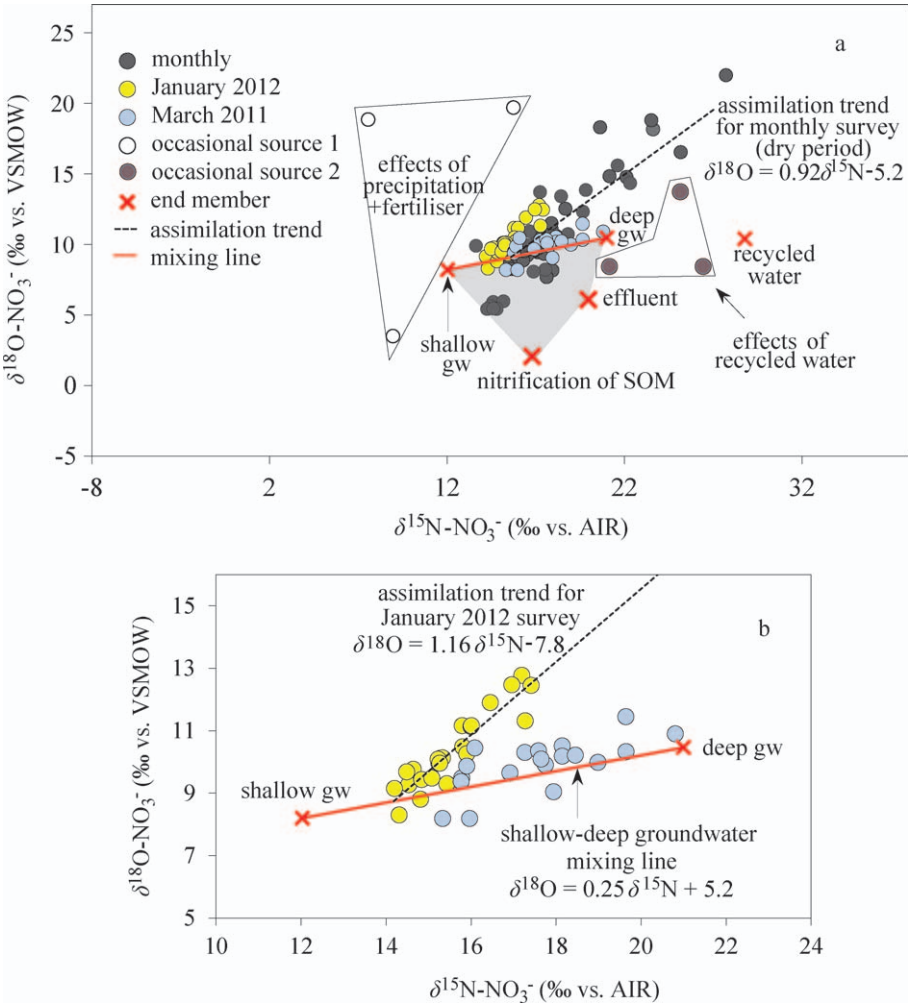

Fig. 8. Relationship between $\delta^{18}O$-NO_3^- and $\delta^{15}N$-NO_3^- to discriminate the possible sources of NO_3^- to the Werribee River estuary. Occasional source 1 represents the $\delta^{15}N$-NO_3^- and $\delta^{18}O$-NO_3^- values of the estuarine NO_3^- that were affected by the $\delta^{15}N$-NO_3^- and $\delta^{18}O$-NO_3^- of precipitation and fertilizer. Occasional source 2 represents the $\delta^{15}N$-NO_3^- and $\delta^{18}O$-NO_3^- values of the estuarine NO_3^- that were affected by the $\delta^{15}N$-NO_3^- and $\delta^{18}O$-NO_3^- of recycled water. (a) All data from monthly and time series surveys are presented. (b) Close-up of the data from the time series surveys.

in the shallow aquifer. The shallow aquifer may be relatively confined and hence more isolated from the effect of recent rainfall.

The monthly survey data exhibited greater spatial and temporal variability than did the two time series surveys. Mixing between shallow and deep groundwater alone is not sufficient to explain the distribution of the estuarine $\delta^{15}N$-NO_3^- below the groundwater mixing line (shaded area in Fig. 8). Deviation of these $\delta^{15}N$-NO_3^- and $\delta^{18}O$-NO_3^- values could be most plausibly attributed to the effect of nitrification on the NH_4^+ derived from SOM and/or mixing with effluent from the sewage treatment plant discharged to the bay.

This explanation is based on the more depleted $\delta^{18}O$-NO_3^- of effluent and nitrification in comparison to that of the groundwaters (Fig. 8). This instance provides a practical example of the advantage of using both $\delta^{15}N$-NO_3^- and $\delta^{18}O$-NO_3^- in distinguishing the sources of NO_3^-. To quantify the relative magnitude of the four potential end members (shallow groundwater, deep groundwater, effluent, and nitrification) with only two isotope system ($\delta^{15}N$-NO_3^- and $\delta^{18}O$-NO_3^-), we used 'Isosource' (Phillips and Gregg 2003). This statistical approach is a powerful method for determining the feasible solutions or bounds of contributions of each source when the number of potential sources exceeds the number of isotopic tracers. While this approach has been widely applied to various environmental studies, for instance, Samborska et al. (2013), Savoye et al. (2012), and Jaschinski et al. (2011), the main concern is the risk of misinterpretation of the feasible solutions as the true solution (Fry 2006). Hence, we have carefully reported the results as a contribution range (minimum and maximum) for each source rather than assuming the mean to represent the actual contribution.

The estuarine samples below the shallow–deep groundwater mixing line were clustered into three groups (A, B, and C) based on the close proximity of the data, and the averages of these groups were used to estimate the possible

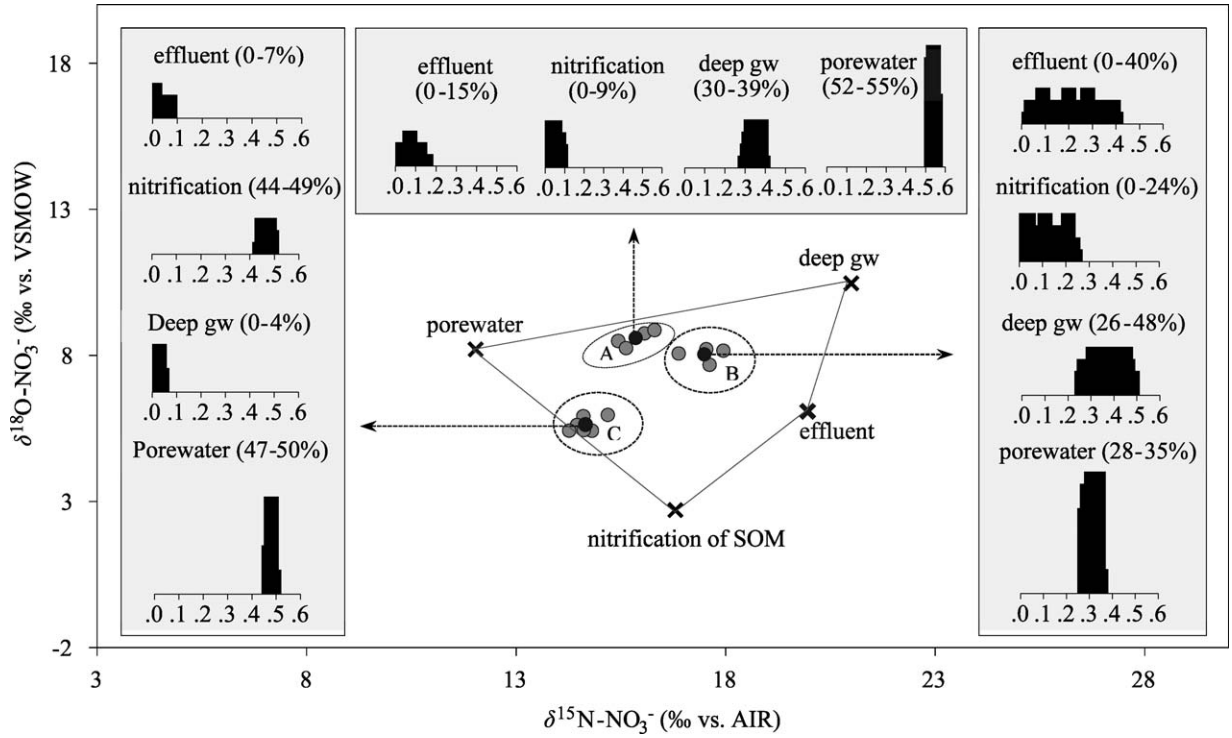

Fig. 9. Mixing polygon for δ^{15}N-NO_3^- and δ^{18}O-NO_3^- signatures of four potential NO_3^- sources for samples that fall below the shallow gw–deep gw isotopic mixing line. Black dots represent the average of δ^{15}N-NO_3^- and δ^{18}O-NO_3^- values of the clustered data: A, B, and C. The averages were used to construct the histograms. Histograms show the distribution of feasible contributions from each source to A, B, and C. Values shown in boxes are maximum and minimum ranges (within first to 99th percentile) of the source contribution to respective data clusters.

contribution of each source to the estuarine NO_3^- (Fig. 9). We found that for all of the sample groups, shallow and/or deep groundwater remained as the primary source. Effluent and nitrification did not appear to have any major effect on group A samples, but effluent could constitute up to 40% of the group B samples, while nitrification could constitute up to 50% of the group C samples. While it is not surprising that both effluent and nitrification of SOM could contribute NO_3^- to the estuary, these are not prominent sources of NO_3^- to the estuary because (1) if such sources were important, we would expect the time series samples to fall below the shallow–deep groundwater mixing line, (2) group B samples were mainly obtained from the mouth of the estuary, more likely demonstrating the local influence of effluent discharged into the bay entering the mouth of the estuary, and (3) group C samples were observed only during wet periods, reflecting the transient nature of this source. If the nitrification rate is assumed to be equal to the sedimentary efflux of NH_4^+ (0.5–1.0 mmol m^{-2} h^{-1}; Table 1), nitrification constitutes a maximum of only $\sim$ 14% of the groundwater-derived NO_3^- fluxes ($\sim$ 7.0 mmol m^{-2} h^{-1}). Hence, nitrification within the estuary is not a major source of NO_3^- to the whole estuary.

Occasional sources of NO_3^- to the estuary—As mentioned in the preceding text, recycled water and precipitation + fertilizer are two occasional sources of NO_3^- to the estuary (Fig. 8). The NO_3^- input from recycled water is supported by the significant correlation ($r^2 = 0.79$, $p < 0.001$, $n = 13$; not shown) between the δ^{15}N-NO_3^- signal observed at W0 and the amount of recycled water being supplied. In addition, the occurrence of anomalously heavy δ^{15}N-NO_3^- in the April 2010 and October 2010 surveys (Fig. 7), during which the monthly supply of recycled water was the highest (up to 850 ML) throughout the survey period, reinforces the contribution of recycled water to estuarine NO_3^- concentrations.

During wet periods, when rainfall exceeded 100 mm (January and February 2011), the depleted δ^{15}N-NO_3^- consistency with an increase in NO_3^- concentration (Fig. 7) suggests the likely influence of surface runoff, which comprised a relatively high percentage of inorganic fertilizer. The effect of total precipitation is also reflected by the relatively heavier δ^{18}O-NO_3^-, indicated by the positive deviation of these data on the δ^{18}O-NO_3^- vs. δ^{15}N-NO_3^- plot (Fig. 8). Although the contribution of these sources is clear and important, we emphasize that these sources are not the controlling end members of the NO_3^- variability in the estuary (as identified by the δ^{18}O-NO_3^- values).

Assimilation: The major transformation process of NO_3^- in the estuary—A conceptual diagram (Fig. 10) is constructed to draw together the effects of different processes on the groundwater-derived NO_3^- in the Werribee River estuary. In the conceptual diagram, the water column of the salt wedge estuary is illustrated to have two distinctive layers: a brackish surface layer and a saline bottom layer.

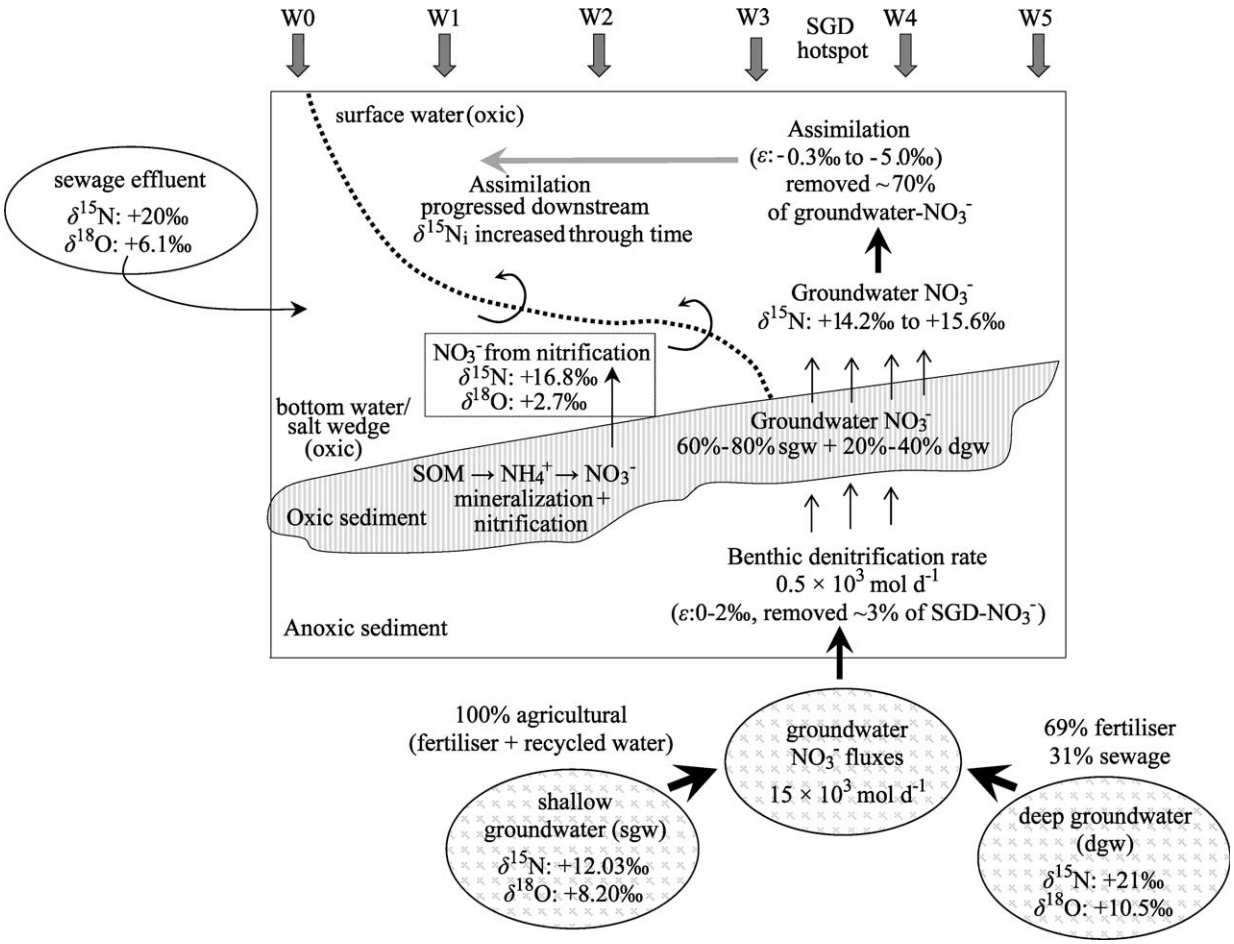

Fig. 10. Conceptual diagram summarizing the sources and transformation processes of NO_3^- to the estuary based on δ^{15}N-NO_3^- and δ^{18}O-NO_3^- values.

Despite the salinity difference between the surface layer and the bottom layer, the estuary remained oxic at all times, with oxygen saturation reaching maximum values of 107% and 92% in the surface and bottom layers, respectively. Based on this oxic status of the water column, we can rule out the possibility of pelagic denitrification. Benthic denitrification also cannot account for the total removal, and the isotopic enrichment, of the groundwater-derived NO_3^-. This contention is based on the low average benthic denitrification rate ($\sim$ 120 μmol m^{-2} h^{-1}) compared to SGD-derived NO_3^- fluxes ($\sim$ 7.0 mmol m^{-2} h^{-1}). Even assuming uniform removal throughout the estuary (surface area of 518,223 m^2), the benthic denitrification rate ($\sim$ 62 mol h^{-1}) only represents about 16% of the SGD-derived NO_3^- flux ($\sim$ 392 mol h^{-1}) based on the SGD hotspot boundary (55,950 m^2).

Hence, assimilation, which imparts a significant isotopic discrimination effect on the residual NO_3^- pool, appears to be the most plausible removal mechanism of the groundwater-derived NO_3^-. The importance of assimilation is substantiated by the simultaneous enrichment of both δ^{15}N-NO_3^- and δ^{18}O-NO_3^- of the remaining NO_3^-, increasing in a 1:1 ratio (Fig 7). If assimilation is the primary removal process of estuarine NO_3^-, the fractionation factor is expected to fall between -6‰ to -13‰ (Kendall et al. 2007). This hypothesis is evaluated via the modeled isotopic behavior of NO_3^- in the water column using closed-system Rayleigh equations (Fry 2006) based on two scenarios. The first scenario considers the spatial and temporal variability of the fractionation process over a monthly timescale and assumes that assimilation of the groundwater-derived NO_3^- occurred throughout the estuary, including the groundwater discharge hotspot, W4. The second scenario considers the variability of the fractionation factor over a shorter timescale and is investigated at the groundwater discharge hotspot using the January 2012 time series field measurements. In both instances, the fraction of NO_3^- reacted (F) was first calculated using Eqs. 3 and 4 as the deviation of NO_3^- concentration from the conservative mixing between bay and groundwater. Nitrate concentrations of the groundwater end member were estimated based on a percentage mixture between shallow and deep groundwater (i.e., sgw : dgw of 3 : 2 for the monthly survey and of 4 : 1 for the January 2012 time series survey) and corrected for the riverine NO_3^- load. Slopes of the relationship between δ^{15}N-NO_3^- and ln(F) are interpreted as the enrichment factor (ε) of the assimilation process based on the Rayleigh equation (Eq. 5).

As indicated in Fig. 11, assimilation accounted for a loss of 66% to 72% [average ln(F) = -0.33 to -0.44] of the

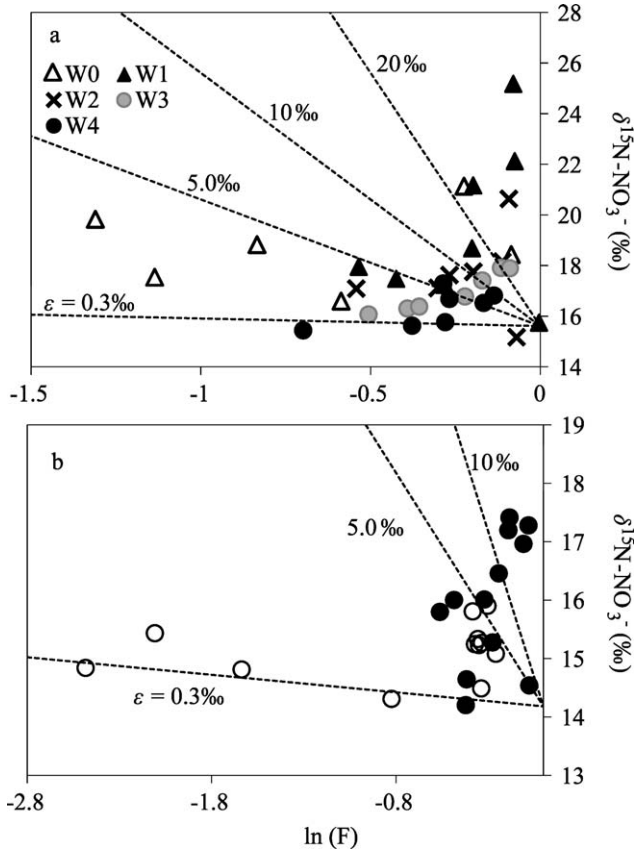

Fig. 11. Relationship between δ^{15}N-NO_3^- and ln(F), where F is the fraction of NO_3^- consumed via assimilation (calculated from Eqs. 3, 4, and 5) for (a) the monthly surveys during the dry period, and (b) the January 2012 time series survey. Dotted lines represent the distribution of δ^{15}N-NO_3^- and ln(F) based on the theoretical enrichment factor (ε) between −0.3‰ to −20‰ and predicted initial δ^{15}N-NO_3^- of + 15.6‰ (monthly survey) and +14.2‰ (time series survey).

groundwater-derived NO_3^-. The isotopic values of the estuarine NO_3^- of the monthly data set displayed enrichment factors between 0.3‰ and 20‰ (average of 10‰), for a few data that exceeded 20‰, which were observed in the lower estuary (W0 and W1). For the January 2012 survey, the majority of the data fall within the modeled ε range of 0.3‰ to 5‰. A higher ε (> 10‰) was observed for the bottom water, which was sampled during high tides, suggesting the expression of heavier initial δ^{15}N-NO_3^-, and was likely to be the effect of sewage from the bay, which was brought riverward by the incoming tide. The influence of sewage-derived NO_3^- also explains the distribution of the monthly data toward the ε values of more than 10‰, which are generally observed at the lower estuary. The overall estimated ε (0‰ to 10‰) falls within the reported values for enrichment factors for field studies in coastal environments (Table 3). The lower estimate (~ 0.3‰ to 5.0‰) of the ε in this study is in close agreement with laboratory culture studies (Needoba et al. 2004) on Chlorophyceae and Cryptophyceae, the dominant phytoplankton species in the Werribee River estuary (J. Sherwood unpubl.). This finding supports our contention that assimilation is the primary consumption process of groundwater-derived NO_3^- in the Werribee River estuary.

In summary, our observations based on δ^{15}N-NO_3^- and δ^{18}O-NO_3^- suggest that groundwater is the dominant source of NO_3^- to the estuary, overiding NO_3^- contributions from other surface sources. Simultaneous application of δ^{15}N-NO_3^- and δ^{18}O-NO_3^- has also enabled us to undertake NO_3^- source apportionment by constraining the percentage contribution of shallow and deep groundwaters—an added advantage of the dual isotopic approach that has not been demonstrated previously. We found that shallow groundwater accounted for at least 60% of the estuarine NO_3^-, while 40% was from deep groundwater. Because the shallow groundwater comprised ~ 100% agricultural sources and deep groundwater consists of 69% sewage and 31% fertilizer (W. W. Wong unpubl.), the dominance of the shallow groundwater means that NO_3^- from the WID is the primary contributor of NO_3^- to the estuary. As such, management strategies should be targeted toward reducing NO_3^- loads from the WID.

Apart from unraveling the sources of NO_3^-, the δ^{15}N-NO_3^- and δ^{18}O-NO_3^- values have also qualitatively highlighted the strong linkages between ephemeral hydrologic controls on NO_3^- variability in the hydrologically complex estuary via continuous time series measurements and quantitatively estimate the importance of assimilation as the major NO_3^--removal process in the estuary. Assimilation removed 66% to 72% of the groundwater-

Table 3. Comparison of the enrichment factor of assimilation, NO_3^- concentration, and δ^{15}N-NO_3^- from field studies in coastal settings.

Study area (estuary)	Surface water [NO_3^-] (μmol L^{-1})	ε (‰)	Surface water δ^{15}N-NO_3^- (‰)	Reference
Yangtze River estuary, China	8 to 80	3*	+0.4 to +6.5	Liu et al. 2009
Elkhorn Slough, California	5 to 400	3 to 10*	+7 to +16	Wankel et al. 2009
Wanquoit Bay, Massachusetts	0 to 50	3 to 7*	−10 to +7	York et al. 2007
Bay of Seine, France	10 to 400	3 to 5†	+1 to +6	Savoye et al. 2003
Auke Bay, Alaska	0 to 26	4†	+6.9‡	Goering et al. 1990
Chesapeake Bay	11 to 22	7†	−0.8 to 5.5	Horrigan et al. 1990
Werribee River estuary, Australia	1 to 500	0.3 to 5*	+8 to +28	This study

* ε was estimated based on δ^{15}N-NO_3^- vs. [NO_3^-].
† ε was estimated based on δ^{15}N-PN vs. δ^{15}N-NO_3^-.
‡ No direct measurement of the surface water δ^{15}N-NO_3^-; estimated from the relationship between δ^{15}N of phytoplankton vs. [NO_3^-].

derived NO_3^- during baseflow periods, with an estimated isotopic enrichment factor of −0.3‰ to −10‰. Overall, the findings of this study suggest that greater emphasis should to be placed upon the role of groundwater when studying the sources of NO_3^- to estuaries and/or other aquatic ecosystems. In addition, δ^{15}N-NO_3^- and d^{18}O-NO_3^- can be considered as alternative tracers to delineate the interaction between surface water and groundwater, specifically in terms of NO_3^- dynamics.

Acknowledgments

We thank Mardiana Ali, Keryn Roberts, Yassir Arafat, and Poh Seng Chee for their help in the field; Daryl Holland for providing the benthic denitrification data; and Ryan Woodland for his assistance with the statistical analysis. We thank the anonymous reviewers for their thoughtful and constructive review of the manuscript.

This work was supported by Melbourne Water Corporation, the Department of Sustainability and Environment, the Environmental Protection Authority Victoria. and an Australian Research Council Grant (LP110100040) to P.L.M.C.

References

Alkhatib, M., M. F. Lehmann, and P. A. Del Giorgio. 2012. The nitrogen isotope effect of benthic remineralization-nitrification-denitrification coupling in an estuarine environment. Biogeosciences **9:** 1633–1646, doi:10.5194/bg-9-1633-2012

American Public Health Association (APHA). 2005. Standard methods for the examination of water and wastewater, 21st ed. American Public Health Association, American Water Works Association, and Water Environment Federation.

Brandes, J. A., A. H. Devol, T. Yoshinari, D. A. Jayakumar, and S. W. A. Naqvi. 1998. Isotopic composition of nitrate in the Central Arabian Sea and Eastern Tropical North Pacific: A tracer for mixing and nitrogen cycles. Limnol. Oceanogr. **43:** 1680–1689, doi:10.4319/lo.1998.43.7.1680

Burnett, W. C., and H. Dulaiova. 2003. Estimating the dynamics of groundwater input into the coastal zone via continuous radon-222 measurements. J. Environ. Radioact. **69:** 21–35, doi:10.1016/S0265-931X(03)00084-5

Casciotti, K. L., D. M. Sigman, M. G. Hastings, J. K. Böhlke, and A. Hilkert. 2002. Measurement of the oxygen isotopic composition of nitrate in seawater and freshwater using the denitrifier method. Anal. Chem. **74:** 4905–4912, doi:10.1021/ac020113w

Commonwealth Scientific and Industrial Research Organisation (CSIRO). 1996. Port Phillip Bay environmental study—the findings 1992–1996. Melbourne Water [Internet]. [accessed 30 April 2011]. http://www.melbournewater.com.au/getinvolved/education/Documents/Port%20Phillip%20Bay%20Environmental%20Study.pdf

Dähnke, K., E. Bahlmann, and K. Emeis. 2008. A nitrate sink in estuaries? An assessment by means of stable nitrate isotopes in the Elbe estuary. Limnol. Oceanogr. **53:** 1504–1511, doi:10.4319/lo.2008.53.4.1504

Dalsgaard, T., and others. 2000. Protocol handbook for NICE—Nitrogen cycling in estuaries: A project under the EU research programme. Silkeborg, Denmark: Marine Science and Technology (MAST III) [Internet]. National Environmental Research Institute, Available from http://www2.dmu.dk/lakeandestuarineecology/nice/nice_handbook.pdf

Dong, L. F., D. B. Nedwell, and A. Stott. 2006. Sources of nitrogen used for denitrification and nitrous oxide formation in sediments of the hypernutrified Colne, the nutrified Humber, and the oligotrophic Conwy estuaries, United Kingdom. Limnol. Oceanogr. **51:** 545–557, doi:10.4319/lo.2006.51.1_part_2.0545

Ellis, P. S., A. M. H. Shabani, B. S. Gentle, and I. D. McKelvie. 2011. Field measurement of nitrate in marine and estuarine waters with a flow analysis system utilizing on-line zinc reduction. Talanta **84:** 98–103, doi:10.1016/j.talanta.2010.12.028

Fry, B. 2006. Stable isotope ecology. Springer.

Galloway, J. N. 2005. The global nitrogen cycle: Past, present and future. Sci. China Series C Life Sci. Chin. Acad. Sci. **48:** 669–677.

Goering, J., V. Alexander, and N. Haubenstock. 1990. Seasonal variability of stable carbon and nitrogen isotope ratios of organisms in a North Pacific Bay. Estuar. Coast. Shelf Sci. **30:** 239–260, doi:10.1016/0272-7714(90)90050-2

Granger, J., D. M. Sigman, M. F. Lehmann, and P. D. Tortell. 2008. Nitrogen and oxygen isotope fractionation during dissimilatory nitrate reduction by denitrifying bacteria. Limnol. Oceanogr. **53:** 2533–2545, doi:10.4319/lo.2008.53.6.2533

Heiskanen, A. S., J. Haapala, and K. Gundersen. 1998. Sedimentation and pelagic retention of particulate C, N and P in the Coastal Northern Baltic Sea. Estuar. Coast. Shelf Sci. **46:** 703–712, doi:10.1006/ecss.1997.0320

Horrigan, S. G., J. P. Montoya, J. L. Nevins, and J. J. McCarthy. 1990. Natural isotopic composition of dissolved inorganic nitrogen in the Chesapeake Bay. Estuar. Coast. Shelf Sci. **30:** 393–410, doi:10.1016/0272-7714(90)90005-C

Jaschinski, S., D. C. Brepohl, and U. Sommer. 2011. Seasonal variation in carbon sources of mesograzers and small predators in an eelgrass community: Stable isotope and fatty acid analyses. Mar. Ecol. Prog. Ser. **431:** 69–82, doi:10.3354/meps09143

Kendall, C., E. M. Elliott, and S. D. Wankel. 2007. Tracing anthropogenic inputs of nitrogen to ecosystems, p. 375–449. *In* R. H. Michener and K. Lajtha [eds.], Stable isotopes in ecology and environmental science. Blackwell Publishing.

Kennish, M. J. 2002. Environmental threats and environmental future of estuaries. Environ. Conserv. **29:** 78–107, doi:10.1017/S0376892902000061

Kroeger, K. D., and M. A. Charette. 2008. Nitrogen biogeochemistry of submarine groundwater discharge. Limnol. Oceanogr. **53:** 1025–1039, doi:10.4319/lo.2008.53.3.1025

Kroopnick, P., and H. Craig. 1972. Atmospheric oxygen: Isotopic composition and solubility fractionation. Science **175:** 54–55, doi:10.1126/science.175.4017.54

Liu, X., Z. Yu, X. Song, and X. Cao. 2009. The nitrogen isotopic composition of dissolved nitrate in the Yangtze River (Changjiang) estuary, China. Estuar. Coast. Shelf Sci. **85:** 641–650, doi:10.1016/j.ecss.2009.09.017

Lourey, M. J., T. W. Trull, and D. M. Sigman. 2003. Sensitivity of δ^{15}N of nitrate, surface suspended and deep sinking particulate nitrogen to seasonal nitrate depletion in the Southern Ocean. Glob. Biogeochem. Cycles **17:** 1081, doi:10.1029/2002GB001973

Mariotti, A., A. Landreau, and B. Simon. 1988. ^{15}N isotope biogeochemistry and natural denitrification process in groundwater: Application to the chalk aquifer of northern France. Geochim. Cosmochim. Acta **52:** 1869–1878, doi:10.1016/0016-7037(88)90010-5

Middelburg, J. J., and J. Nieuwenhuize. 2001. Nitrogen isotope tracing of dissolved inorganic nitrogen behavior in tidal estuaries. Estuar. Coast. Shelf Sci. **53:** 385–391, doi:10.1006/ecss.2001.0805

Needoba, J. A., D. M. Sigman, and P. J. Harrison. 2004. The mechanism of isotope fractionation during algal nitrate assimilation as illuminated by the $^{15}N/^{14}N$ of intracellular nitrate. J. Phycol. **40:** 517–522, doi:10.1111/j.1529-8817.2004.03172.x

Nielsen, L. P. 1992. Denitrification in sediment determined from nitrogen isotope pairing. FEMS Microbiol. Ecol. **86:** 357–362.

Nixon, S. W. 1995. Coastal marine eutrophication: A definition, social causes, and future concerns. Ophelia **41:** 199–219.

Null, K. A., and others. 2012. Submarine groundwater discharge-derived nutrient loads to San Francisco Bay: Implications to future ecosystem changes. Estuar. Coasts **35:** 1299–1315, doi:10.1007/s12237-012-9526-7

Paerl, H. W. 1997. Coastal eutrophication and harmful algal blooms: Importance of atmospheric deposition and groundwater as "new" nitrogen and other nutrient sources. Limnol. Oceanogr. **42:** 1154–1165, doi:10.4319/lo.1997.42.5_part_2.1154

———, J. L. Pinckney, J. M. Fear, and B. L. Peierls. 1998. Ecosystem responses to internal and watershed organic matter loading: Consequences for hypoxia in the eutrophying Neuse River Estuary, North Carolina, USA. Mar. Ecol. Prog. Ser. **166:** 17–25, doi:10.3354/meps166017

Phillips, D. L., and J. W. Gregg. 2003. Source partitioning using stable isotopes: Coping with too many sources. Oecologia **136:** 261–269, doi:10.1007/s00442-003-1218-3

Quay, P. D., D. O. Wilbur, J. E. Richey, A. H. Devol, R. Benner, and B. R. Forsberg. 1995. The $^{18}O:^{16}O$ of dissolved oxygen in rivers and lakes in the Amazon Basin: Determining the ratio of respiration to photosynthesis rates in freshwaters. Limnol. Oceanogr. **40:** 718–729, doi:10.4319/lo.1995.40.4.0718

Samborska, K., S. Halas, and S. H. Bottrell. 2013. Sources and impact of sulphate on groundwaters of Triassic carbonate aquifers, Upper Silesia, Poland. J. Hydrol. **486:** 136–150, doi:10.1016/j.jhydrol.2013.01.017

Santos, I. R., W. C. Burnett, T. Dittmar, I.G.N.A. Suryaputra, and J. Chanton. 2009. Tidal pumping drives nutrient and dissolved organic matter dynamics in a Gulf of Mexico subterranean estuary. Geochim. Cosmochim. Acta **73:** 1325–1339, doi:10.1016/j.gca.2008.11.029

———, R. N. Peterson, B. D. Eyre, and W. C. Burnett. 2010. Significant lateral inputs of fresh groundwater into a stratified tropical estuary: Evidence from radon and radium isotopes. Mar. Chem. **121:** 37–48, doi:10.1016/j.marchem.2010.03.003

Savoye, N., A. Aminot, P. Tréguer, M. Fontugne, N. Naulet, and R. Kérouel. 2003. Dynamics of particulate organic matter $\delta^{15}N$ and $\delta^{13}C$ during spring phytoplankton blooms in a macrotidal ecosystem (Bay of Seine, France). Mar. Ecol. Prog. Ser. **255:** 27–41, doi:10.3354/meps255027

———, and others. 2012. Origin and composition of particulate organic matter in a macrotidal turbid estuary: The Gironde Estuary, France. Estuar. Coast. Shelf Sci. **108:** 16–28, doi:10.1016/j.ecss.2011.12.005

Sebilo, M., B. Mayer, M. Grably, D. Billion, and A. Mariotti. 2004. The use of the 'ammonium diffusion' method for $\delta^{15}N$-NH_4^+ and $\delta^{15}N$-NO_3^- measurements: Comparison with other techniques. Environ. Chem. **1:** 99–103, doi:10.1071/EN04037

Sigman, D. M., K. L. Casciotti, M. Andreani, C. Barford, M. Galanter, and J. K. Böhlke. 2001. A bacterial method for the nitrogen isotopic analysis of nitrate in seawater and freshwater. Anal. Chem. **73:** 4145–4153, doi:10.1021/ac010088e

———, R. Robinson, A. N. Knapp, A. Van Geen, D. C. McCorkle, J. A. Brandes, and R. C. Thunell. 2003. Distinguishing between water column and sedimentary denitrification in the Santa Barbara Basin using the stable isotopes of nitrate. Geochem. Geophys. Geosyst. **4:** 1040, doi:10.1029/2002GC000384

Sigman, O. M., M. A. Altabet, D. C. McCorkle, R. Francois, and G. Fischer. 1999. The $\delta^{15}N$ of nitrate in the Southern Ocean: Consumption of nitrate in surface waters. Glob. Biogeochem. Cycles **13:** 1149–1166, doi:10.1029/1999GB900038

Slomp, C. P., and P. Van Cappellen. 2004. Nutrient inputs to the coastal ocean through submarine groundwater discharge: Controls and potential impact. J. Hydrol. **295:** 64–86, doi:10.1016/j.jhydrol.2004.02.018

Wankel, S. D., C. Kendall, C. A. Francis, and A. Paytan. 2006. Nitrogen sources and cycling in the San Francisco Bay estuary: A nitrate dual isotopic composition approach. Limnol. Oceanogr. **51:** 1654–1664, doi:10.4319/lo.2006.51.4.1654

———, ———, and A. Paytan. 2009. Using nitrate dual isotopic composition $\delta^{15}N$ and $\delta^{18}O$ as a tool for exploring sources and cycling of nitrate in an estuarine system: Elkhorn Slough, California. J. Geophys. Res. G Biogeosci. **114:** G01011, doi:10.1029/2008jg000729

Wong, W. W., M. R. Grace, I. Cartwright, M. B. Cardenas, P. B. Zamora, and P. L. M. Cook. 2013. Dynamics of groundwater-derived nitrate and nitrous oxide in a tidal estuary from radon mass balance modeling. Limnol. Oceanogr. **58:** 1689–1706, doi:10.4319/lo.2013.58.5.1689

Xue, D., and others. 2009. Present limitations and future prospects of stable isotope methods for nitrate source identification in surface- and groundwater. Wat. Res. **43:** 1159–1170, doi:10.1016/j.watres.2008.12.048

York, J. K., G. Tomasky, I. Valiela, and D. J. Repeta. 2007. Stable isotopic detection of ammonium and nitrate assimilation by phytoplankton in the Waquoit Bay estuarine system. Limnol. Oceanogr. **52:** 144–155, doi:10.4319/lo.2007.52.1.0144

Associate editor: H. Maurice Valett

Received: 11 October 2013
Accepted: 01 June 2014
Amended: 02 June 2014